

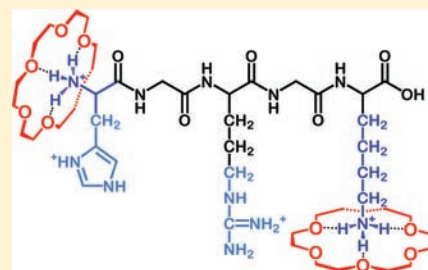
# Structural and Energetic Effects in the Molecular Recognition of Protonated Peptidomimetic Bases by 18-Crown-6

Yu Chen and M. T. Rodgers\*

Department of Chemistry, Wayne State University, Detroit, Michigan 48202, United States

**S** Supporting Information

**ABSTRACT:** Absolute 18-crown-6 (18C6) affinities of nine protonated peptidomimetic bases are determined using guided ion beam tandem mass spectrometry techniques. The bases (B) included in this work are mimics for the n-terminal amino group and the side chains of the basic amino acids, i.e., the favorable sites for binding of 18C6 to peptides and proteins. Isopropylamine is chosen as a mimic for the n-terminal amino group, imidazole and 4-methylimidazole are chosen as mimics for the side chain of histidine (His), 1-methylguanidine is chosen as a mimic for the side chain of arginine (Arg), and several primary amines including methylamine, ethylamine, n-propylamine, n-butylamine, and 1,5-diamino pentane as mimics for the side chain of lysine (Lys). Theoretical electronic structure calculations are performed to determine stable geometries and energetics for neutral and protonated 18C6 and the peptidomimetic bases, as well as the proton bound complexes comprised of these species, (B)H<sup>+</sup>(18C6). The measured 18C6 binding affinities of the Lys side chain mimics are larger than the measured binding affinities of the mimics for Arg and His. These results suggest that the Lys side chains should be the preferred binding sites for 18C6 complexation to peptides and proteins. Present results also suggest that competition between Arg or His and Lys for 18C6 is not significant. The mimic for the n-terminal amino group exhibits a measured binding affinity for 18C6 that is similar to or greater than that of the Lys side chain mimics. However, theory suggests that binding to n-terminal amino group mimic is weaker than that to all of the Lys mimics. These results suggest that the n-terminal amino group may compete with the Lys side chains for 18C6 complexation.



## INTRODUCTION

Structure–function relationships are well established for biological polymers and, in particular, proteins. As a result, studies aimed at the characterization and improved understanding of the three-dimensional structure of proteins and the intra- and intermolecular interactions that stabilize their structures and complexes are ubiquitous throughout the biological and chemical disciplines. X-ray crystallography<sup>1</sup> and NMR spectroscopy<sup>2,3</sup> are well-established analytical techniques for protein structure elucidation. However, NMR requires a large quantity of the protein in a specific solvent, while X-ray crystallography requires sample crystallization, which can be difficult to achieve. Mass spectrometry (MS) has become an increasingly important tool for protein structure determination due to its speed, sensitivity, and specificity.<sup>4–6</sup>

A variety of MS approaches have been used to characterize protein structure and intra- and intermolecular protein interactions. One approach is H/D exchange,<sup>7–13</sup> in which labile hydrogen atoms along the protein backbone and side chains undergo replacement with deuterium at differing exchange rates. The exchange rates are primarily determined by the accessibility of solvent to the backbone and side chain hydrogen atoms, as well as intramolecular hydrogen bonding. Protein structural information is correlated to the H/D exchange reaction rates. Therefore, H/D exchange is an efficient technique for studying changes in protein structure

and dynamics due to ligand binding, protein modification, and protein–protein interactions.

Chemical cross-linking is another approach employed for the study of protein three-dimensional structures and protein–protein interactions.<sup>14–22</sup> Cross-linking reactions are generally carried out using homo- or heterobifunctional cross-linking reagents, binding to specific functional targets, to impose a distance constraint on the respective protein side chains. The length and conformation of the cross-linking reagent are controlled; therefore, intramolecular cross-linking can provide further insight into how proteins fold. In contrast, intermolecular cross-linking facilitates the determination of reactive components and protein surface contacts.

Beauchamp, Julian, and co-workers have developed a third approach, selective noncovalent adduct protein probing (SNAPP)<sup>23–32</sup> using crown ethers to selectively bind to the side chains of basic amino acids to explore protein structure and folding states. The SNAPP method utilizes noncovalent recognition of amino acid residues, and in particular lysine (Lys) residues, to facilitate rapid identification and characterization of protein sequence, structure and conformational changes, and provides information key to understanding functional behavior in biological systems at the molecular level. In this approach, 18C6 was selected as the protein side

Received: October 31, 2011

Published: December 23, 2011

chain tag because of its enzymelike specificity for Lys side chains. The extent of 18C6 adduction to Lys side chains is determined by the number of accessible Lys side chains, i.e., those that are not involved in intramolecular interactions such as hydrogen bonds or salt bridges. Intramolecular interactions generally prevent the attachment of 18C6 and are directly correlated to the structure of the protein. Therefore, binding of 18C6 can be employed as a sensitive probe of protein structure. Because the number of 18C6 ligands that bind to a protein can be easily determined by MS due to the large mass shift (264 Da per 18C6 ligand bound), information relevant to protein folding information under varying solution conditions can be extrapolated.

The use of molecular recognition of crown ethers by various protein sequences and structures has also been pursued in other groups. Brodbelt and co-workers reported a method using 18C6 derivatized with a chromophore, to study the fragmentation patterns of peptides.<sup>33</sup> The chromophore tag noncovalently binds to a Lys side chain via the 18C6 moiety. The chromophore facilitates peptide fragmentation by absorbing UV irradiation and transferring it to the peptide via intramolecular vibrational redistribution (IVR). Schneider and co-workers developed a strategy, using crown ethers as scaffolds for protein surface target recognition to explore protein folding and the mechanism of ligand binding. They designed a peptide receptor with 18C6 at one binding site for interaction with the peptide N-terminus and a peralkylammonium group as the other binding site for interaction with the C-terminus, via binding to the zwitterionic form of the unprotected tripeptide, Gly-Trp-Gly, to develop a peptide differentiation method based on length, amino acid composition, sequence, and the configuration of peptides and proteins.<sup>34,35</sup> Griebenow and co-workers colyophilized subtilisin Carlsberg, a protein digesting enzyme, with 18C6 in organic solvent to investigate how enzyme structure and stability are correlated to catalytic properties.<sup>36</sup> They found that colyophilization of subtilisin with 18C6 substantially improves enzyme activity in organic solvents. They concluded that the active site structure is locally preserved by the presence of the crown ether. Exposure to organic solvents leads to the release of the crown ether but the active site structure remains intact, leading to activation of the enzyme.

The charged amino acids, arginine (Arg), histidine (His), Lys, glutamic acid (Glu), and aspartic acid (Asp) offer the best targets for molecular recognition of specific side chains in peptides or proteins. As a result of the structural similarity of the acidic amino acids, aspartate, and glutamate, which differ only in the number of methylene groups in the side chain, the acidic amino acids are difficult to distinguish. The basic amino acids, Lys, His, and Arg, offer the possibility of achieving specificity due to the very different chemical functionalities of the basic side chains.

Lysine is one of the most common amino acids in proteins, and it is almost always found at protein surfaces. Welfle and co-workers used maleic anhydride covalently bound to Lys residues to determine the relative reactivity of Lys residues in HIV-1 capsid protein p24 (rp24).<sup>37</sup> They concluded that an epitope binding affinity for antibody strongly increased after maleic anhydride modification of the Lys residue of rp24 due to the induced change in protein conformation. D'Ambrosio and co-workers investigated the structure of porcine aminoacylase 1 (ACY1), a zinc-binding metalloenzyme using acetylation with acetic anhydride.<sup>38</sup> MALDI-MS analyses found 8 of the 17 Lys

residues acetylated indicating that these residues are solvent-exposed.

Although the protonated side chain of Lys has been shown to be the primary binding site for 18C6 complexation, the protonated side chains of His, Arg, and the n-terminal amino group may also compete for 18C6. Therefore, accurate thermochemical information regarding the binding between 18C6 and the basic amino acids may provide insight into the selectivity of the complexation process. However, very limited thermochemical data has thus far been reported in the literature. Mautner used the kinetic method to determine the proton affinities (PAs) of polyethers and crown ethers.<sup>39</sup> In this method, the competitive dissociation of proton bound dimers comprised of two distinct bases, the base of interest and a reference base of known PA was examined. The base that exhibits the greater fragment ion abundance (protonated base) is presumed to have a greater PA. The PA of 18C6 was determined to be  $923.0 \pm 8.4$  kJ/mol based on comparison to two reference bases, 1,2-diazine and pyridine. The PA of 18C6 was also determined by Kebarle and co-workers.<sup>40</sup> In their study, they used ammonia as a reference base to extrapolate the PA of 18C6 as  $961.5 \pm 8.4$  kJ/mol.

In the present study, absolute 18C6 affinities of nine protonated peptidomimetic bases are determined using guided ion beam tandem mass spectrometry techniques. Peptidomimetic bases that serve as models for the n-terminal amino group and the side chains of Lys, His, and Arg are examined here. Isopropylamine (IPA) is chosen as a mimic for the n-terminal amino group, imidazole (IMID) and 4-methylimidazole (4MeIMID) are chosen as mimics for the side chain of His, 1-methylguanidine (MGD) is chosen as a mimic for the side chain of Arg, and several primary amines including methylamine (MA), ethylamine (EA), n-propylamine (NPA), n-butylamine (NBA), and 1,5-diamino pentane (DAP) as mimics for the side chain of Lys, as shown in Figure 1. The

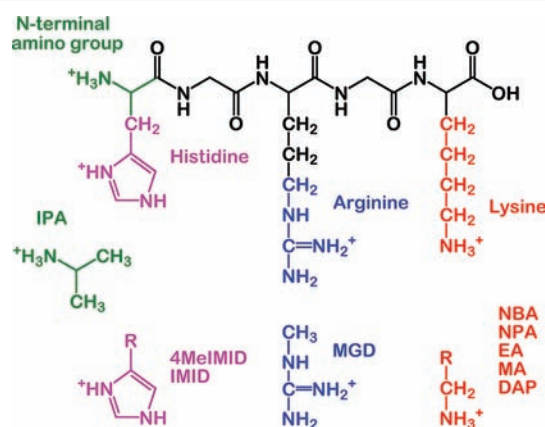


**Figure 1.** Structures of the peptidomimetic nitrogen bases examined as mimics for the n-terminal amino group and the side chains of the basic amino acids, histidine, arginine, and lysine.

energy-dependent cross sections for collision-induced dissociation (CID) of the protonated peptidomimetic base–18C6 complexes are analyzed using methods previously developed that explicitly include the effects of the kinetic and internal energy distributions of the reactants, multiple ion-neutral collisions, and the kinetics of unimolecular dissociation. Absolute (B)H<sup>+</sup>–18C6 bond dissociation energies (BDEs)

for all nine (B)H<sup>+</sup>(18C6) complexes are derived and compared to theoretical estimates for these BDEs computed here.

## EXPERIMENTAL SECTION

**General Procedures.** Cross sections for CID of nine protonated peptidomimetic base–18C6 complexes, (B)H<sup>+</sup>(18C6) with Xe, where B = IMID, 4MeIMID, MA, EA, NPA, NBA, IPA, DAP, and MGD are measured using a guided ion beam tandem mass spectrometer that has been described in detail previously.<sup>41</sup> The (B)H<sup>+</sup>(18C6) complexes are generated by electrospray ionization (ESI) as described below. The ions are effusively sampled from the source region, focused, accelerated, and focused into a magnetic sector momentum analyzer for mass analysis. Mass-selected ions are decelerated to a desired kinetic energy and focused into an octopole ion guide. The octopole passes through a static gas cell containing Xe at low pressure (~0.05–0.20 mTorr) to ensure that multiple ion-neutral collisions are improbable. The octopole acts as an efficient trap for ions in radial direction.<sup>42</sup> Therefore, loss of scattered reactant and product ions in the octopole region is almost entirely eliminated. Xe is used as the collision gas because it is heavy and polarizable and therefore leads to more efficient kinetic to internal energy transfer in the CID process. Products and remaining reactant ions drift to the end of the octopole, are focused into a quadrupole mass filter for mass analysis, and are subsequently detected with a secondary electron scintillation detector and standard pulse counting techniques.

**Ion Source and Interface.** Ions are generated using a home-built ESI source similar in design to that developed by Moison et al.<sup>43</sup> 18C6 and the relevant peptidomimetic base, B, are dissolved in a 50:50 by volume MeOH:H<sub>2</sub>O mixture to produce a solution that is ~0.2 mM in each species. The solution is delivered to a 35 gauge stainless steel ESI needle via a syringe pump at a flow rate of ~1.0 μL/min. The ESI needle is biased at 1.7–2.0 kV for the complexes examined here. Ions emanating from the spray are transferred into the vacuum region through a stainless steel capillary with a 0.03" inner diameter (ID) biased at 20–50 V, and heated to 90–130 °C. The capillary is ~4.0" long and its exit is flush with the first plate of the rf ion funnel.

The rf ion funnel, similar to the design developed by Smith and co-workers,<sup>44,45</sup> is a focusing device that facilitates efficient transfer of ions from the high pressure source region to the low pressure region of the mass spectrometer. The ion funnel consists of 88 0.020" thick brass ring electrodes. Each electrode is separated by a 0.020" thick Teflon sheet. The first 44 electrodes have a constant ID of 1.000", while the latter 44 electrodes have IDs that decrease from 1.000" to 0.094" to form a linear taper. A linear dc gradient is applied across the ion funnel by applying a dc voltage to the first and last plates of the ion funnel with a resistor chain connecting all intervening plates. The entrance plate is biased at ~20 V, while the exit plate is held at ~2 V for the systems investigated here. Adjacent electrodes receive equal and opposite phases of an rf signal with peak-to-peak voltage in the range between 10 and 30 V, and is operated at a frequency in the range between 0.6 and 1.2 MHz. This oscillating field on the plates and the tapering of the lenses focuses ions radially to the center of the ion funnel.

A jet disrupter (JD), a 0.25" diameter metal disk, is located ~1.0" from the entrance of the ion funnel to prevent large droplets from the spray from depositing downstream on the hexapole ion guide. The JD is biased at 15–25 V. A dc-only injection lens with a 0.140" I.D. follows the last plate of the ion funnel to prevent ions that have entered the hexapole from diffusing back upstream toward the ion funnel. The injection lens is biased at a voltage between the final ion funnel plate and the hexapole dc voltage, which is typically held at ground potential.

Ions emanating from the ion funnel are thermalized in the hexapole ion guide by collisions with the background gases. The hexapole is operated in the rf only mode with a peak to peak voltage of ~300 V and a frequency of 5.5 MHz. Therefore, the ions pass through the hexapole region primarily by diffusion.

**Data Handling.** Ion intensities are converted to absolute cross sections using a Beer's law analysis as described previously.<sup>46</sup>

Uncertainties in the pressure measurement and the length of interaction region lead to ±20% uncertainties in the cross section magnitudes. Relative uncertainties are approximately ±5%.

Ion kinetic energies in the laboratory frame,  $E_{\text{lab}}$ , are converted to energies in the center-of-mass frame,  $E_{\text{CM}}$ , using the formula  $E_{\text{CM}} = E_{\text{lab}} m/(m + M)$ , where  $M$  and  $m$  are the masses of the ionic and neutral reactants, respectively. All energies reported below are in the center-of-mass frame unless otherwise noted. The absolute zero and distribution of the ion kinetic energies are determined using an octopole ion guide as a retarding potential analyzer as previously described.<sup>46</sup> The distribution of kinetic energies is nearly Gaussian with a full width at half-maximum (fwhm) between 0.2 and 0.5 eV (lab) for these experiments. The uncertainty in the absolute energy scale is ±0.05 eV (lab).

Because multiple ion-neutral collisions can influence the shape of CID cross sections, particularly in the threshold region, the CID cross section for each complex was measured twice at three nominal pressures (0.05, 0.1, 0.2 mTorr). Data free from pressure effects are obtained by extrapolating to zero pressure of the Xe reactant, as described previously.<sup>47</sup> Therefore, the cross sections subjected to thermochemical analysis are the result of single bimolecular encounters.

**Theoretical Calculations.** To obtain stable geometries, vibrational frequencies, and energetics for neutral and protonated 18C6 and the peptidomimetic bases as well as the proton bound complexes comprised of these species, (B)H<sup>+</sup>(18C6), theoretical calculations were performed using HyperChem<sup>48</sup> and the Gaussian 03<sup>49</sup> and 09<sup>50</sup> suites of programs. Neutral and protonated 18C6 exhibit numerous stable low-energy structures, therefore a simulated annealing methodology using HyperChem and the AMBER force field was used to generate starting structures for higher level optimization. All structures determined within 30 kJ/mol of the lowest-energy structure were optimized using density functional methods.

Geometry optimizations for the neutral and protonated peptidomimetic bases as well as the proton bound (B)H<sup>+</sup>(18C6) complexes were performed using density functional theory at the B3LYP/6-31G\* level.<sup>51,52</sup> Vibrational analyses of the geometry-optimized structures were performed to determine the vibrational frequencies of the optimized species for use in modeling of the CID data. The frequencies calculated were scaled by a factor of 0.9804.<sup>53</sup> The scaled vibrational frequencies and rotational constants are listed in Tables 1S and 2S of the Supporting Information. Because all systems examined here involve hydrogen bonds, we also performed geometry optimization of the ground-state structures of the nine (B)H<sup>+</sup>(18C6) complexes at the B3LYP/6-311+G(d,p) level of theory, adding a polarized p function on the hydrogen atoms and a diffuse function on heavy atoms, to assess the dependence of the theoretical results on the level of theory employed for geometry optimization. Single-point energy calculations were performed at the B3LYP/6-311+G(2d,2p), MP2(full)/6-311+G(2d,2p), and M06/6-311+G(2d,2p) levels of theory using the B3LYP/6-31G\* and B3LYP/6-311+G(d,p) optimized geometries, respectively. To obtain accurate BDEs, zero-point energy (ZPE), and basis set super position error (BSSE) corrections are included in the computed BDEs using the counterpoise approach.<sup>54,55</sup>

**Thermochemical Analysis.** The threshold regions of the CID cross sections are modeled using an empirical threshold energy law, eq 1

$$\sigma(E) = \sigma_0 \sum_i g_i (E + E_i - E_0)^n / E \quad (1)$$

where  $\sigma_0$  is an energy independent scaling factor,  $E$  is the relative translational energy of the reactants,  $E_0$  is the threshold for reaction of the ground electronic and ro-vibrational state, and  $n$  is an adjustable parameter that describes the efficiency of kinetic to internal energy transfer.<sup>56</sup> The summation is over the ro-vibrational states of the reactant ions,  $i$ , where  $E_i$  is the excitation energy of each state, and  $g_i$  are the populations of those states ( $\sum g_i = 1$ ). The relative reactivity of

all ro-vibrational states, as reflected by  $\sigma_0$  and  $n$ , is assumed to be equivalent.

The density of the ro-vibrational states is determined using the Beyer–Swinehart algorithm,<sup>57–59</sup> and the relative populations,  $g_p$ , are calculated for a Maxwell–Boltzmann distribution at 298 K, the temperature of the reactants. Vibrational frequencies and rotational constants of the reactant (B)H<sup>+</sup>(18C6) complexes are determined as described in the Theoretical Calculations section. The average internal energy at 298 K of the (B)H<sup>+</sup>(18C6) complexes and their primary CID products, H<sup>+</sup>(B) and 18C6, are included in Table 1S of the Supporting Information. The calculated frequencies are scaled by  $\pm 10\%$  to estimate the sensitivity of our analysis to the deviations from the true frequencies as suggested by Pople et al.<sup>60,61</sup> The corresponding change in the average vibrational energy is taken to be an estimate of one standard deviation of the uncertainty in vibrational energy (Table 1S).

All CID reactions that occur faster than the experimental time scale,  $\sim 10^{-4}$  s, should be observed. However, as the complexity of the reactant (B)H<sup>+</sup>(18C6) ions increases, there is an increased probability that the CID reaction will not take place within the experimental time window. Once the lifetime of the energized molecule (EM) approaches this limit, the CID threshold shifts to higher energies, resulting in a kinetic shift. Therefore, statistical theories for unimolecular dissociation were included in the analysis, specifically Rice–Ramsperger–Kassel–Marcus (RRKM) theory, as described in detail elsewhere<sup>62,63</sup> to quantify and correct for the kinetic shift. This requires sets of ro-vibrational frequencies appropriate for the EM and the transition states (TSs) leading to dissociation. The TSs are expected to be loose and productlike and modeled using the ro-vibrational frequencies of the products for these systems. This treatment corresponds to a phase space limit (PSL) in which the TS occurs at the centrifugal barrier for dissociation as described in detail elsewhere.<sup>62</sup> The ro-vibrational frequencies of the EMs and TSs of the (B)H<sup>+</sup>(18C6) complexes are given in Tables 1S and 2S of the Supporting Information.

The model represented by eq 1 is expected to be appropriate for translationally driven reactions<sup>64</sup> and has been found to reproduce cross sections well in previous studies of CID processes.<sup>65–68</sup> The model is convoluted with the kinetic and internal energy distributions of the reactants, and a nonlinear least-squares analysis of the data is performed to give optimized values for the parameters  $\sigma_0$ ,  $E_0$ , and  $n$ . The errors associated with the measurement of  $E_0$  are estimated from the range of threshold values determined for the zero-pressure-extrapolated data sets for each complex, variations associated with uncertainties in the vibrational frequencies, and the error in the absolute energy scale, 0.05 eV (lab). For analyses that include the RRKM lifetime analysis, the uncertainties in the reported  $E_0$ (PSL) values also include the effects of increasing and decreasing the time assumed available for dissociation ( $\sim 10^{-4}$  s) by a factor of 2.

Equation 1 explicitly includes the internal energy of the reactant ion,  $E_i$ . All energy available is treated statistically because the ro-vibrational energy of the reactants is redistributed throughout the (B)H<sup>+</sup>(18C6) complex upon interaction with Xe. Because the CID processes examined here are simple noncovalent bond cleavage reactions, the  $E_0$ (PSL) values determined from analysis with eq 1 can be equated to 0 K BDEs.<sup>69,70</sup> The accuracy of the thermochemistry obtained by this modeling procedure has been verified for many systems by comparing values derived from other experimental techniques and to ab initio calculations. Absolute BDEs in the range from  $\sim 10$  to 400 kJ/mol have been accurately determined using threshold collision-induced dissociation (TCID) techniques.<sup>71</sup>

## RESULTS

### Cross Sections for Collision-Induced Dissociation.

Experimental cross sections were obtained for the interaction of Xe with nine (B)H<sup>+</sup>(18C6) complexes, where B = IMID, 4MeIMID, MA, EA, NPA, NBA, IPA, DAP, and MGD. Figure 2 shows representative data for the (NBA)H<sup>+</sup>(18C6) complex. Experimental cross sections for the other (B)H<sup>+</sup>(18C6)

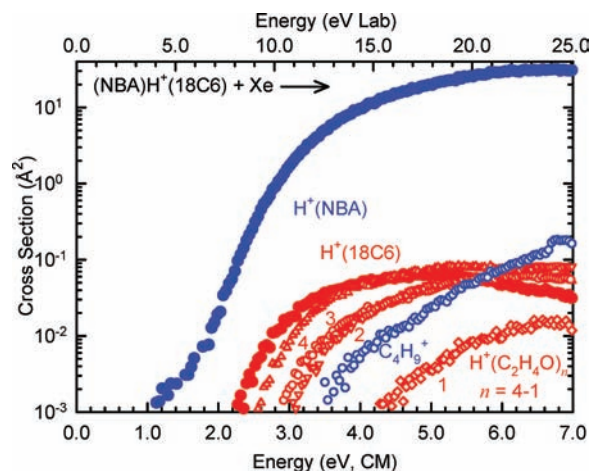
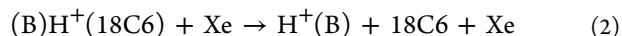
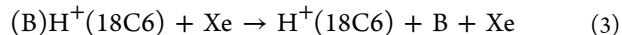


**Figure 2.** Cross sections for collision-induced dissociation of the (NBA)H<sup>+</sup>(18C6) complex with Xe as a function of kinetic energy in the center-of-mass frame (lower x-axis) and laboratory frame (upper x-axis). Data are shown for a Xe pressure of 0.2 mTorr.

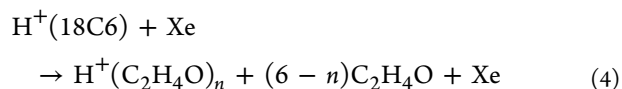
complexes are shown in Figure 1S of the Supporting Information. The most favorable process for all complexes is loss of an intact 18C6 ligand in the CID reactions 2.



Loss of the neutral base, B to produce H<sup>+</sup>(18C6) was also observed as a minor product in competition with H<sup>+</sup>(B) for all complexes except those where B = MGD and DAP, CID reactions 3.

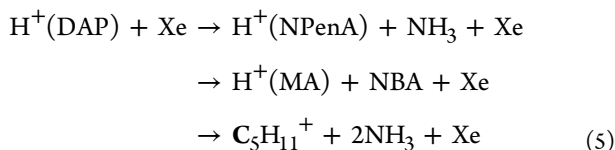


The magnitude of the H<sup>+</sup>(18C6) product cross section is the largest for the (IMID)H<sup>+</sup>(18C6) complex, a factor of 4 higher than that in the (NBA)H<sup>+</sup>(18C6) and (IPA)H<sup>+</sup>(18C6) systems, and a factor of 25 higher than that in the (4MeIMID)H<sup>+</sup>(18C6) system. The same trend was also found for the branching ratio between H<sup>+</sup>(18C6) and H<sup>+</sup>(B) in these systems: 4MeIMID < IPA  $\approx$  NBA < IMID. In contrast, the relative thresholds between H<sup>+</sup>(18C6) and H<sup>+</sup>(B) in these systems follow the reverse trend. The difference between the threshold for H<sup>+</sup>(18C6) and H<sup>+</sup>(B) in the (IMID)H<sup>+</sup>(18C6) system is the smallest,  $\sim 0.6$  eV, indicating that competition between the formation of H<sup>+</sup>(18C6) and H<sup>+</sup>(B) in this system is the most significant. As a result, the magnitude of the H<sup>+</sup>(18C6) product cross section in the (IMID)H<sup>+</sup>(18C6) system is the greatest. The difference between the H<sup>+</sup>(18C6) and H<sup>+</sup>(B) threshold increases to  $\sim 1.1$  eV for complexes involving NBA and IPA and increases to  $\sim 1.5$  eV for the complex involving 4MeIMID. At elevated energies, products corresponding to the sequential dissociation of H<sup>+</sup>(18C6) were also observed for all complexes, reactions 4, except the (4MeIMID)H<sup>+</sup>(18C6) complex.



It is likely that such sequential fragmentation processes also occur in the (4MeIMID)H<sup>+</sup>(18C6) system, but that the signal-to-noise in those experiments was not sufficient to differentiate the H<sup>+</sup>(C<sub>2</sub>H<sub>4</sub>O)<sub>n</sub> fragments from background noise ( $\sim 10^{-3}$  Å<sup>2</sup>). For the (DAP)H<sup>+</sup>(18C6) and (MGD)H<sup>+</sup>(18C6) complexes,

the  $\text{H}^+(18\text{C}6)$  competitive dissociation pathway was not observed due to the relatively large difference in the PAs of the bases and 18C6. At elevated energies, fragments such as 1-pentanamine (NPenA) and guanidine (GD) corresponding to sequential dissociation of  $\text{H}^+(\text{DAP})$  and  $\text{H}^+(\text{MGD})$  were observed, reactions 5 and 6.



More detailed analyses of the fragments corresponding to the sequential dissociation of  $\text{H}^+(18\text{C}6)$  and  $\text{H}^+(\text{B})$  were not pursued here and thus will not be discussed further.

**Theoretical Results.** Theoretical structures for the  $(\text{B})\text{H}^+(18\text{C}6)$  complexes as well as the neutral and protonated bases and 18C6 were calculated as described in the Theoretical Calculations Section. The ground-state structures of the  $(4\text{MeIMID})\text{H}^+(18\text{C}6)$ ,  $(\text{MGD})\text{H}^+(18\text{C}6)$ , and  $(\text{NBA})\text{H}^+(18\text{C}6)$  complexes are shown in Figure 3, while the

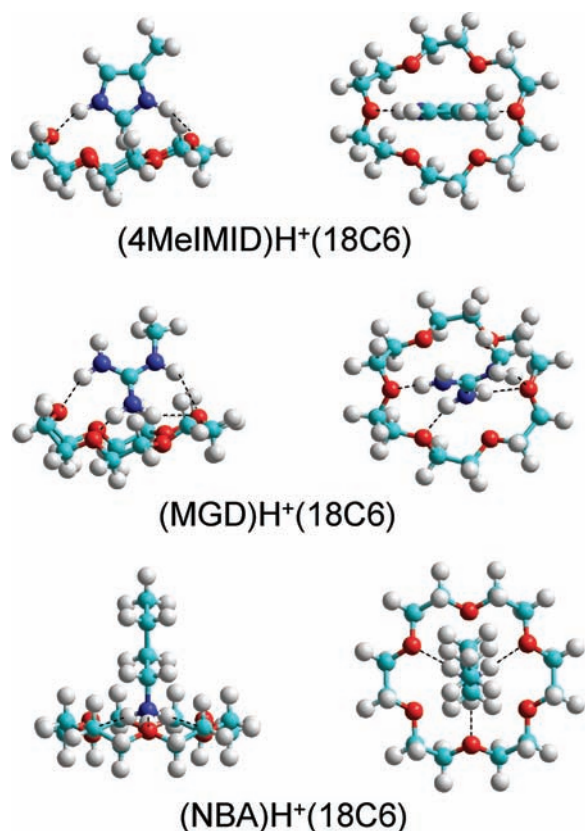


**Figure 3.** B3LYP/6-31G\* optimized geometries of the ground-state conformers of the  $(4\text{MeIMID})\text{H}^+(18\text{C}6)$ ,  $(\text{MGD})\text{H}^+(18\text{C}6)$ , and  $(\text{NBA})\text{H}^+(18\text{C}6)$  complexes.

structures for the other six  $(\text{B})\text{H}^+(18\text{C}6)$  complexes are shown in Figure 2S of the Supporting Information. Results for the stable low-energy conformations of the neutral and protonated bases are shown in Figure 3S. Structures of several representative low-energy conformations of neutral and protonated 18C6 are shown in Figures 4S and 5S, respectively.

The  $(\text{B})\text{H}^+ - 18\text{C}6$  BDEs at 0 K calculated at the MP2(full), B3LYP, and M06 levels of theory using a 6-311+G(2d,2p) basis set for both levels of geometry optimization B3LYP/6-31G\* and B3LYP/6-311+G(d,p) including ZPE and BSSE corrections, are listed in Table 1, while values listed in Table 3S provide details of the ZPE and BSSE corrections. Comparison of the measured and calculated values suggests that the MP2(full) results are most reliable and that surprisingly the agreement is very slightly better for structures optimized at the B3LYP/6-31G\* level. Therefore, the following discussion will focus on the geometries and relative energies calculated at MP2(full)/6-311+G(2d,2p)//B3LYP/6-31G\* level of theory unless otherwise specified.

**18C6.** The ground-state conformation of neutral 18C6 is of  $C_i$  symmetry; four of its six ether oxygen atoms are directed inward from the ether backbone, while the other two are directed outward as shown in Figure 4S. A weak intramolecular C–H...O interaction helps stabilize the ground-state conformer. A stable conformer with  $D_{3d}$  symmetry was also found that lies 14.8 kJ/mol higher in energy than the ground-state structure (Figure 4S). In this conformation, each of the oxygen atoms are directed inward from the ether backbone, forming a nucleophilic cavity for very favorable interaction with guest cations. These structures are consistent with the lowest-energy conformers identified by Feller and Glendening.<sup>72,73</sup> In their study, the  $D_{3d}$  conformer was computed to lie 18.4 kJ/mol (RHF/6-31+G\*//RHF/6-31+G\*) and 22.6 kJ/mol (MP2/6-31+G\*//RHF/6-31+G\*) higher in energy than the ground-state conformation.

In the ground-state conformation of  $\text{H}^+(18\text{C}6)$ , the proton binds to an O atom and is stabilized by an O1...H...O3 hydrogen bond (Figure 5S). The ground-state of  $\text{H}^+(18\text{C}6)$  exhibits a boatlike conformation. A relatively flat conformation of  $\text{H}^+(18\text{C}6)$  with the proton stabilized between the O1 and O3 oxygen atoms was also found that lies 30.6 kJ/mol higher in energy than the ground-state structure. The conformer where the proton binds to an oxygen atom and maintains the  $\sim D_{3d}$  symmetry of the 18C6 backbone lies 65.6 kJ/mol higher in energy than the ground-state structure.

**Peptidomimetic Bases.** Details of the optimized geometries for the ground-state conformations of the neutral and protonated bases are provided in the Supporting Information in Figure 2S. The preferred site of protonation for all bases is to the lone pair of electrons on the nitrogen atom. For IMID and 4MeIMID, the proton binds at the N3 position of the imidazole ring to form a conformer with  $C_{2v}$  and  $C_s$  symmetry, respectively. In the ground-state structure of  $\text{H}^+(\text{IPA})$ ,  $\text{H}^+(\text{MA})$ ,  $\text{H}^+(\text{EA})$ ,  $\text{H}^+(\text{NPA})$ , and  $\text{H}^+(\text{NBA})$ , the proton binds to the amino group. The hydrocarbon backbones of the ground-state conformers of  $\text{H}^+(\text{EA})$ ,  $\text{H}^+(\text{NPA})$ , and  $\text{H}^+(\text{NBA})$  exhibit zigzag conformations.  $\text{H}^+(\text{DAP})$  can form an eight membered ring conformer that is stabilized by a hydrogen bonding interaction between the protonated and neutral amino groups. The extended zigzag conformer in which the proton is attached to a single amino group is 69.2 kJ/mol less favorable than the ground-state conformer. For MGD, the proton could bind to the primary or secondary amine or the primary imine to form a stable protonated conformer. The most favorable protonation site is the imine nitrogen atom, which is 148.9 and 150.1 kJ/mol more favorable than the primary and secondary amine binding sites, respectively.

**$(\text{B})\text{H}^+(18\text{C}6)$  Complexes.** In the ground-state conformations of the  $(\text{B})\text{H}^+(18\text{C}6)$  complexes, the proton binds to the

Table 1. (B)H<sup>+</sup>–18C6 Bond Dissociation Enthalpies at 0 K in kJ/mol<sup>a</sup>

B	TCID <sup>b</sup>	MP2 (full)	M06	B3LYP
4MeIMID	167.6 (6.9)	167.1 (167.7)	162.7 (164.0)	136.8 (136.7)
MGD	174.3 (6.3)	165.7 (165.6)	167.7 (166.5)	133.6 (134.5)
IMID	175.0 (9.3)	177.1 (178.1)	174.8 (176.2)	148.2 (148.4)
DAP	185.8 (9.8)	177.8 (179.6)	183.8 (185.4)	142.0 (145.2)
NBA	223.8 (9.5)	247.4 (248.1)	256.4 (253.0)	210.5 (211.7)
NPA	224.2 (9.3)	248.1 (248.8)	255.1 (254.6)	212.4 (213.4)
EA	233.2 (10.4)	250.8 (251.3)	258.9 (258.3)	216.7 (217.6)
MA	238.0 (10.6)	259.8 (261.2)	266.4 (266.9)	234.6 (235.6)
IPA	238.3 (10.1)	240.8 (241.6)	248.6 (249.4)	199.0 (200.1)
AEU/MAD <sup>c</sup>	9.1 ± 1.5	12.1 ± 9.7 (12.5 ± 10.1)	15.8 ± 13.3 (15.4 ± 12.9)	25.2 ± 14.6 (24.2 ± 14.4)

<sup>a</sup>Single-point energies are calculated using the 6-311+G(2d,2p) basis set and the geometries optimized at the B3LYP/6-31G\* level of theory. Single-point energies calculated using the 6-311+G(2d,2p) basis set and the geometries optimized at the B3LYP/6-311+G(d,p) level of theory are listed in parentheses. <sup>b</sup>Uncertainties are listed in parentheses. <sup>c</sup>Average experimental uncertainty (AEU) and mean absolute deviation (MAD) between theory and experiment. MADs using geometries optimized at B3LYP/6-311+G(d,p) basis set are listed in parentheses.

Table 2. Threshold Dissociation Energies at 0 K and Entropies of Activation at 1000 K of (B)H<sup>+</sup>(18C6) Complexes<sup>a</sup>

B	$\sigma_0^b$	$n^b$	$E_0$ (eV) <sup>c</sup>	$E_0$ (PSL) (eV) <sup>b</sup>	Kinetic Shift (eV)	$\Delta S$ (PSL) (J mol <sup>-1</sup> K <sup>-1</sup> )
4MeIMID	117.5 (5.9)	0.8 (0.1)	3.08 (0.08)	1.74 (0.07)	1.34	69 (5)
MGD	94.5 (4.2)	0.9 (0.1)	3.03 (0.1)	1.81 (0.07)	1.22	109 (4)
IMID	61.9 (4.8)	1.0 (0.1)	3.12 (0.11)	1.81 (0.10)	1.31	85 (4)
DAP	94.6 (10.4)	1.3 (0.1)	3.52 (0.1)	1.93 (0.10)	1.59	113 (4)
NBA	68.9 (5.7)	1.0 (0.1)	4.58 (0.13)	2.32 (0.10)	2.26	109 (4)
NPA	3.5 (0.4)	1.2 (0.1)	4.36 (0.04)	2.32 (0.10)	2.04	116 (4)
EA	4.8 (0.4)	1.3 (0.1)	4.40 (0.10)	2.42 (0.11)	1.98	115 (4)
MA	44.6 (4.3)	1.3 (0.1)	4.57 (0.08)	2.47 (0.11)	2.10	103 (4)
IPA	62.5 (4.2)	0.8 (0.1)	4.65 (0.14)	2.47 (0.10)	2.18	123 (2)

<sup>a</sup>Present results, uncertainties are listed in parentheses. <sup>b</sup>Average values for loose PSL transition state. <sup>c</sup>No RRKM analysis.

peptidomimetic base to form a protonated structure very similar to that of the isolated protonated base that interacts with 18C6 via N–H···O hydrogen bonds. The preferred site of proton binding remains the base even when the PA of 18C6 exceeds that of the base. The conformation of 18C6 in these complexes bears great similarity to the  $D_{3d}$  structure of the neutral crown with a nucleophilic cavity in the center for interaction with the protonated base.

In the ground-state conformations of the (IPA)H<sup>+</sup>(18C6), (DAP)H<sup>+</sup>(18C6), (MA)H<sup>+</sup>(18C6), (EA)H<sup>+</sup>(18C6), (NPA)H<sup>+</sup>(18C6) and (NBA)H<sup>+</sup>(18C6) complexes (Figures 3 and 2S), the proton binds to the nitrogen atom of the base, resulting in a protonated amino group that interacts with 18C6 via three nearly ideal (i.e., nearly linear) N–H···O hydrogen bonds. The conformation of 18C6 in these complexes bears great similarity to the  $D_{3d}$  structure of the neutral crown with a nucleophilic cavity in the center for the interaction with the protonated base. Complexation to the protonated base causes the 18C6 cavity to contract, resulting in the oxygen to center-of-mass distance to decrease from 2.880 Å in the  $D_{3d}$  conformation of neutral 18C6 to 2.860 Å for (IPA)H<sup>+</sup>(18C6), 2.857 Å for (DAP)H<sup>+</sup>(18C6) and (NBA)H<sup>+</sup>(18C6), 2.854 Å for (NPA)H<sup>+</sup>(18C6) and (EA)H<sup>+</sup>(18C6), and 2.847 Å for (MA)H<sup>+</sup>(18C6) in the ground-state conformations of these complexes. Complexation to 18C6 also induces electron redistribution from the methylene groups toward the oxygen atoms as evidenced by an increase in the Mulliken charges on the oxygen (–) and carbon (+) atoms in the (B)H<sup>+</sup>(18C6) complexes as compared to free 18C6. Another stable conformer was found for the (DAP)H<sup>+</sup>(18C6) system that lies

11.7 kJ/mol higher in energy than the ground-state conformation. In this excited conformer, H<sup>+</sup>(DAP) bears similarity to the ground-state ring structure, where the two amino groups share the proton and interact with the O1 and O4 atoms of 18C6 via two N–H···O hydrogen bonds instead of three as in the ground-state conformer, as shown in Figure 6S of the Supporting Information.

For the (IMID)H<sup>+</sup>(18C6) and (4MeIMID)H<sup>+</sup>(18C6) complexes, the proton binds to the neutral base to form H<sup>+</sup>(IMID) and H<sup>+</sup>(4MeIMID), which bind to a distorted  $D_{3d}$  conformer of 18C6 via two N–H···O hydrogen bonds similar to the excited ring conformer of (DAP)H<sup>+</sup>(18C6). The O1 and O4 atoms of 18C6 are tilted above the nearly planar ring structure forming hydrogen bonds with the hydrogen atoms of the secondary amines. Another low-energy conformer that lies 3.3 and 2.5 kJ/mol higher in energy, respectively, is found for both the (IMID)H<sup>+</sup>(18C6) and (4MeIMID)H<sup>+</sup>(18C6) systems as shown in Figure 6S of the Supporting Information. Compared to the ground-state structures, these conformers differ primarily in the conformations of 18C6, which are flattened somewhat relative to the ground-state conformers. For the (MGD)H<sup>+</sup>(18C6) system, protonated MGD binds to a distorted  $D_{3d}$  conformer of 18C6 via four N–H···O hydrogen bonds to the O1, O2, and O4 (2) atoms. A stable conformer of H<sup>+</sup>(MGD) where the proton is bound to the primary amine also binds to 18C6 to form a stable complex, as shown in Figure 6S of the Supporting Information. However, this latter structure is 43.4 kJ/mol less stable than the ground-state conformer. 18C6 exhibits an approximately  $D_{3d}$  conformation where the six oxygen atoms are oriented toward the interior of

the ring and interact with the primary amine H atoms via three N–H···O hydrogen bonds.

**Threshold Analysis.** The model of eq 1 was used to analyze the thresholds for reactions 2 in nine (B)H<sup>+</sup>(18C6) complexes. The results of these analyses are provided in Table 2. Representative results are shown in Figure 4 for the

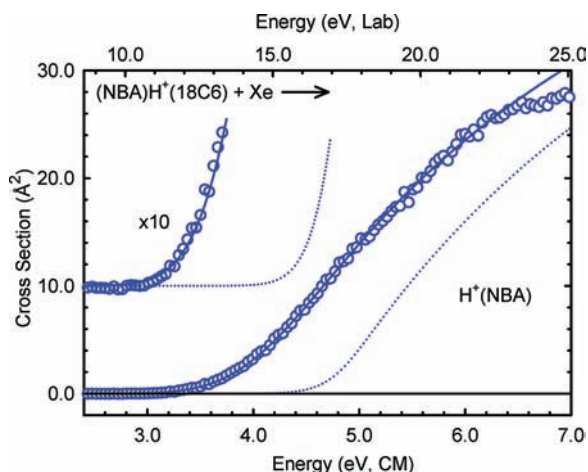


**Figure 4.** Zero-pressure-extrapolated cross section for the H<sup>+</sup>(NBA) primary CID product of the (NBA)H<sup>+</sup>(18C6) complex in the threshold region. The solid lines show the best fit of the data using eq 1 convoluted over the ion and neutral kinetic and internal energy distributions. The dotted line shows the model cross section in the absence of experimental kinetic energy broadening for reactants with an internal energy corresponding to 0 K.

(NBA)H<sup>+</sup>(18C6) complex. The analyses for the other eight (B)H<sup>+</sup>(18C6) complexes are shown in Figure 7S of the Supporting Information. In all cases, the experimental cross sections for reactions 2 are accurately reproduced using a loose PSL TS model.<sup>62</sup> Previous work has shown that this model provides the most accurate assessment of the kinetics shifts for CID process for electrostatically bound ion–molecule complexes.<sup>74–82</sup> Good reproduction of the data is obtained over energy ranges exceeding 3.0 eV and cross section magnitudes of at least a factor of 100. Table 2 also lists  $E_0$  values obtained without including the RRKM lifetime analysis. Comparison of these values with the  $E_0$ (PSL) values shows that the kinetic shifts are the largest for the most strongly bound systems, such that the kinetic shift for the (MA)H<sup>+</sup>(18C6), (EA)H<sup>+</sup>(18C6), (NPA)H<sup>+</sup>(18C6), (NBA)H<sup>+</sup>(18C6), and (IPA)H<sup>+</sup>(18C6) complexes vary between 1.98 and 2.26 eV. No simple correlation among these systems is found as the strength of binding decreases, while the number of modes available increases, with the size of B. The kinetic shift decreases for the (DAP)H<sup>+</sup>(18C6) complex to 1.59 eV, and becomes even smaller, 1.34 to 1.22 eV, for the (4MeIMID)H<sup>+</sup>(18C6), (IMID)H<sup>+</sup>(18C6), and (MGD)H<sup>+</sup>(18C6) complexes. These trends are consistent with expectations that the observed kinetic shift should directly correlate with the density of states of the activated complex at threshold, which increases with energy and the number of modes available to the system.

The entropy of activation,  $\Delta S^\ddagger$ , is a measure of the looseness of the TS and the complexity of the system. It is determined from the molecular parameters used to model the EM and TS for dissociation as listed in Table 1S and 2S. The  $\Delta S^\ddagger$ (PSL) values at 1000 K are listed in Table 2 and vary between 69 to 123 J/K mol across the these systems. These values are

consistent with the noncovalent nature of the binding in these systems. The  $\Delta S^\ddagger$ (PSL) values are the smallest for the complexes to IMID and 4MeIMID, 69 and 85 J/K mol, where only two hydrogen bonds are cleaved in the CID process, and larger for the remaining complexes 103 to 123 J/K mol, where three or four hydrogen bonds are broken.

**Conversion from 0 to 298 K.** To allow comparison to commonly employed experimental conditions, we convert the 0 K bond energies determined here to 298 K bond enthalpies and free energies. The enthalpy and entropy conversions are calculated using standard formulas (assuming harmonic oscillator and rigid rotor models) and vibrational and rotational constants determined for the B3LYP/6-31G\* optimized geometries, which are given in Table 1S and 2S. Table 4S lists 0 and 298 K enthalpy, free energy, and enthalpic and entropic corrections for all systems experimentally determined. Enthalpic and entropic corrections are determined by  $\pm 10\%$  variation in all vibrational frequencies and additionally by  $\pm 50\%$  variation in the N–H···O frequencies associated with the noncovalent binding in the (B)H<sup>+</sup>(18C6) complexes.

## DISCUSSION

**Comparison of Theory and Experiment.** The measured and calculated 18C6 binding affinities of IMID, 4MeIMID, MA, EA, NPA, NBA, IPA, DAP, and MGD at 0 K are summarized in Table 1. The agreement between MP2(full)/6-311+G-(2d,2p)//B3LYP/6-31G\* theory and experiments is illustrated in Figure 5. The mean absolute deviation (MAD) between

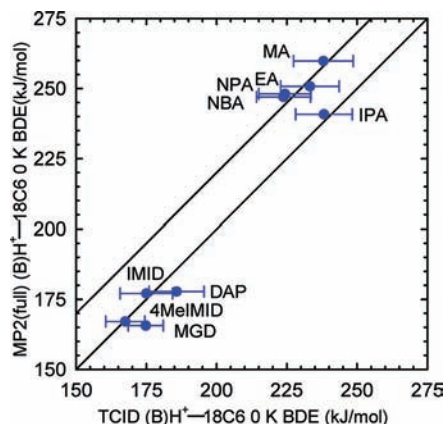


**Figure 5.** Theoretical versus experimental (B)H<sup>+</sup>–18C6 0 K BDEs. Theoretical BDEs determined from single point energy calculations at the MP2(full)/6-311+G(2d,2p) level of theory including ZPE and BSSE corrections.

theory and experiment for all nine complexes is  $12.1 \pm 9.7$  kJ/mol. For the IMID, 4MeIMID, IPA, DAP, and MGD systems, the measured BDEs exhibit excellent agreement with MP2(full) theory with a MAD of  $4.4 \pm 3.8$  kJ/mol. Although a nice linear correlation between the TCID measured and calculated (B)H<sup>+</sup>–18C6 BDEs is found for the MA, EA, NPA, and NBA systems, MP2(full) theory systematically overestimates the BDEs in these complexes by  $21.7 \pm 2.9$  kJ/mol.

The BDEs calculated using M06 theory are consistent with those calculated using MP2(full) theory with deviations between 2 and 8 kJ/mol across these systems. The MAD between M06/6-311+G(2d,2p)//B3LYP/6-31G\* theory and experiments is slightly poorer than for MP2 results,  $15.8 \pm 13.3$  kJ/mol. The BDEs calculated using M06 theory excluding the

Lys mimics exhibit excellent agreement with the measure BDEs with a MAD similar to that found for MP2(full) theory,  $4.9 \pm 4.0$  kJ/mol. However, for the MA, EA, NPA, and NBA systems, M06 theory overestimates the BDEs by almost 8 kJ/mol more than MP2(full) theory,  $29.4 \pm 3.0$  kJ/mol. M06 theory reproduces the MP2(full) observed trends in the binding and achieves a similar, albeit reduced, accuracy for the energetics of these systems, but requires significantly less computing time. Thus, M06 is potentially suitable for describing the energetics of larger related hydrogen bound systems, where computational effort becomes increasingly important.

The agreement between B3LYP theory and the measured BDEs is less satisfactory with a MAD of  $25.2 \pm 14.6$  kJ/mol. B3LYP theory systematically underestimates the measured BDEs for the systems, IMID, 4MeIMID, MGD, DAP, and IPA by  $36.4 \pm 7.2$  kJ/mol. For the MA, EA, NPA, and NBA systems, B3LYP theory underestimates the BDEs by  $11.3 \pm 5.6$  kJ/mol. Indeed for these systems B3LYP theory performs better than MP2(full) theory and may be suitable for describing the binding to primary amines.

As described in the Theoretical Calculations section, geometry optimizations were also performed at B3LYP/6-311+G(d,p) level of theory. The additional polarization function on the hydrogen atoms and diffuse function on the heavy atoms does not dramatically alter the optimized geometry, suggesting that the B3LYP/6-31G\* theory is sufficient to describe the structures of these complexes. In addition, the MP2(full)/6-311+G(2d,2p) BDEs for the structures optimized with the extended basis set changed by less than 1.8 kJ/mol in all systems. In fact, the MAD between MP2(full) theory and experiment actually degrades slightly,  $12.5 \pm 10.1$  kJ/mol versus  $12.1 \pm 9.7$  kJ/mol. The M06/6-311+G(2d,2p) BDEs for the structures optimized with the extended basis set changed by less than 3.4 kJ/mol in all systems. The MAD between M06 theory and experiment improves slightly to  $15.4 \pm 12.9$  kJ/mol (versus  $15.8 \pm 13.3$  kJ/mol). The B3LYP/6-311+G(2d,2p) BDEs for the structures optimized with the extended basis set changed by less than 3.2 kJ/mol in all systems. The MAD between B3LYP theory and experiment improves slightly to  $24.2 \pm 14.4$  kJ/mol (versus  $25.2 \pm 14.6$  kJ/mol). Less than 1 kJ/mol change on average suggesting that the additional cost of the calculations using the larger basis set is not justified.

**Trends in the 18C6 Binding Affinities.** The measured  $(B)H^+-18C6$  BDEs determined here follow such order:  $IPA \geq MA > EA > NPA \geq NBA > DAP > IMID \geq MGD > 4MeIMID$ . The interactions of 18C6 with IPA, MA, EA, NPA, NBA, and DAP all involve three nearly ideal N–H...O hydrogen bonds, which result in the strongest noncovalent interactions between 18C6 and the bases investigated here. 18C6 interacts with MGD via four less than ideal (nonlinear) hydrogen bonds with three oxygen atoms to form a low symmetry conformer. 4MeIMID and IMID interact with 18C6 via two nonideal hydrogen bonds to alternate oxygen atoms (O1 and O4) to form relatively more weakly bound complexes. These trends in the  $(B)H^+-18C6$  BDEs confirm that the geometry even more importantly than the number of hydrogen bonding interactions, is critical to the strong binding necessary for molecular recognition. The trends in the measured and computed  $(B)H^+-18C6$  BDEs differ somewhat. Theory overestimates the strength of binding to the primary alkyl amines, MA, EA, NPA, and NBA, whereas values for all of the other peptidomimetic bases are within experimental error of

the measured values. This discrepancy is not well understood, but is not the result of the basis set size used for optimization as discussed in the previous section.

**Binding Sites of Amino Acid Side Chains.** Julian and Beauchamp applied the SNAAP method to exploit noncovalent interactions between crown ethers and the side chains of the amino acids in peptides and proteins. Their results suggest that 18C6 exhibits a strong binding preference for the side chain of Lys residues. In the study by Julian and Beauchamp,<sup>23</sup> a mixture of NBA, guanidine (GD), and IMID was sprayed with 18C6. They observed that the  $(NBA)H^+(18C6)$  complex completely dominates the spectrum and is the base peak (100% relative abundance), while the relative intensity of  $(GD)H^+(18C6)$  and  $(IMID)H^+(18C6)$  is 3.5% and 1%, respectively. Although 18C6 exhibits a binding preference for Lys side chains, the side chains of Arg, His, and the n-terminal amino group may serve as competitive binding sites for 18C6 complexation. This result is consistent with the trends in the measured binding affinities examined here. Our measure BDEs suggest that the 18C6 affinity for the Lys mimics is  $\sim 50$  kJ/mol higher than that for the His and Arg mimics. Therefore, the competition between the Lys residues and His or Arg residues for 18C6 is not severe. Based on the measured CID thresholds, IPA exhibits a greater binding affinity for 18C6 than MA, EA, NPA and NBA. Therefore, the n-terminal amino group could serve as a favorable alternative binding site for 18C6. The X-ray study of Krestov and co-workers suggests that steric interactions with the n-terminal amino acid side chain could constrain its complexation to 18C6.<sup>83</sup> They found that the “depth of penetration” of the ammonium group into the 18C6 cavity for complexation exhibits a significant difference between diglycine and dialanine. The ammonium group in diglycine is much closer to the crown than that of dialanine during complexation. Steric interactions with the methyl side chain in proximity to the amino group in dialanine do not allow 18C6 to approach as closely and therefore bind as strongly. Thus, the 18C6 binding affinity of the n-terminal amino group should depend on the nature of the side chain. Binding should be the strongest when glycine is the n-terminal amino acid and should decrease with increasing size/polarizability of the side chain. Thus, the ability of the n-terminal amino group to compete with the Lys side chains will depend upon the identity of the n-terminal amino acid.

**Measured BDEs versus Polarizability of the Bases.** As discussed above, the measured BDEs for the primary alkyl amine bases MA, EA, NPA, and NBA deviate systematically from the MP2(full)/6-311+G(2d,2p)//B3LYP/6-31G\* calculated BDEs by  $21.7 \pm 2.9$  kJ/mol. The measure BDEs exhibit a reverse linear correlation with the calculated polarizability of the bases as illustrated in Figure 6a. Theoretical calculations indicate that the binding between 18C6 and the bases involves N–H...O hydrogen bonds (or proton-lone pair electron interactions). Therefore, the strength of binding between 18C6 and the bases should be controlled by the nature of the interactions, ion–dipole and ion-induced dipole interactions. The polarizability of MA is  $3.6 \text{ \AA}^3$ , increases to  $5.5 \text{ \AA}^3$  for EA, to  $7.3 \text{ \AA}^3$  for NPA, and to  $9.1 \text{ \AA}^3$  for NBA. The more polarizable bases bind the proton more strongly and distribute the excess charge more evenly throughout the protonated base resulting in greater stabilization. The reduced charge on the protons of the amino group leads to weaker binding to 18C6.

The reverse linear correlation between the measured BDEs and the calculated polarizability of the bases was also observed

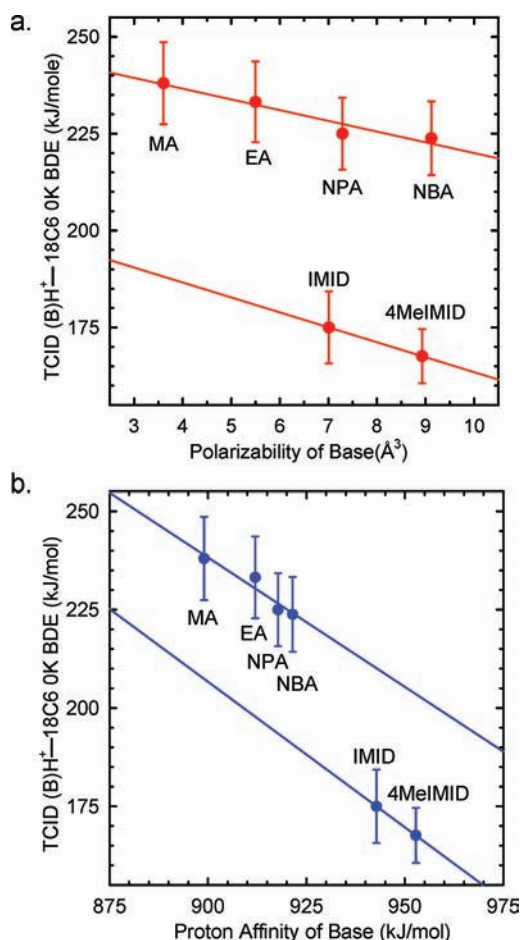


**Figure 6.** Measured (B)H<sup>+</sup>-18C6 BDEs at 0 K (kJ/mol) versus PBE1PBE calculated polarizability of B, where B = MA, EA, NPA, NBA, IMID and 4MeIMID (a). Measured (B)H<sup>+</sup>-18C6 BDEs at 0 K (kJ/mol) versus PA of B, where B = MA, EA, NPA, NBA, IMID and 4MeIMID (b). PA values taken from the NIST Webbook.<sup>85</sup>

for the IMID and 4MeIMID systems, also shown in Figure 6a. The polarizability of IMID is 7.0 Å<sup>3</sup> and increases to 8.9 Å<sup>3</sup> for 4MeIMID. In contrast, the measured (IMID)H<sup>+</sup>-18C6 BDE is 175.0 kJ/mol and decreases to upon 4-methylation of IMID to 167.6 kJ/mol. The correlation line between measured BDEs and the calculated polarizability for the two groups of bases are highly parallel, suggesting that the effects of additional methylene groups are additive. Each additional methylene group contributes to a decrease in the measured BDE by ~5 kJ/mol, and increases the polarizability by ~1.8 Å<sup>3</sup> for both the primary amine and imidazolic bases.

**Measured BDEs versus PA of Bases.** Because the nitrogen bases investigated in this study involve different types of hydrogen bonding interactions with 18C6, the correlation between the proton affinity (PA) of the base and the measured BDEs are examined among bases that exhibit similar binding geometries to 18C6.

Among the Lys mimics, MA, EA, NPA, and NBA, the measured 18C6 binding affinity exhibits a reverse linear correlation with the PA of these bases, as shown in Figure 6b. The PA of NBA is 921.5 kJ/mol, decreases to 917.8 kJ/mol for NPA, 912.0 kJ/mol for EA, and 899.0 kJ/mol for MA.<sup>84</sup> In contrast, the measured (B)H<sup>+</sup>-18C6 BDEs increase from 223.8 kJ/mol for NBA to 224.2 kJ/mol for NPA, 233.2 kJ/mol for EA and 238.0 kJ/mol for MA. This reverse linear correlation was

previously explained based on the N-H bond lengths and the charge retained on the amino protons. Bases with higher PAs bind the proton tighter and lead to weaker interactions with 18C6, resulting in lower dissociation thresholds.

As discussed above, the PAs of the primary amines are anticorrelated with the 18C6 binding affinities. The analogous correlation was also observed between IMID and 4MeIMID, as shown in Figure 6b. The PA of 4MeIMID is 952.8 kJ/mol, ~10 kJ/mol greater than that of IMID.<sup>84</sup> In contrast, the threshold for loss of 18C6 is 7.4 kJ/mol lower for 4MeIMID than that of IMID.

The reverse correlation between PA and the measured (B)H<sup>+</sup>-18C6 BDEs was also found for the MGD containing system. Although there is no PA reported in the literature, MGD is expected to exhibit a higher PA than all of the other bases based on MP2(full) and B3LYP calculations. MP2(full) theory finds that the PA of MGD exceeds that of all of the other bases examined here by 23.2 to 108.1 kJ/mol, whereas B3LYP theory finds slightly larger differences, 31.8 to 120.7 kJ/mol, respectively. In addition, Arg is known to be the most basic amino acid. Therefore, MGD as the mimic of Arg, is expected to exhibit a higher PA than all of the other mimics examined. MGD exhibits a much weaker binding interaction with 18C6 as compared to the MA, EA, NPA, NBA, and IPA systems as a result of the substantial PA difference relative to the other systems, and the very nonideal hydrogen bonding interactions in the (MGD)H<sup>+</sup>(18C6) complex.

Although DAP exhibits different interactions with 18C6 as compared to IPA and MGD, the reverse trend between measured BDEs and PA still loosely holds. DAP has a PA of 999.6 kJ/mol, 75.8 kJ/mol higher than that of IPA. Therefore, the measured BDE for DAP is expected to be lower than the n-terminal amino group mimic. Although the PA of MGD has not been reported, MP2(full) calculations suggest that the PA of DAP is 23.2 kJ/mol lower than that of MGD. Therefore, DAP is expected to exhibit a higher affinity for 18C6 than MGD. This reverse correlation was also observed for these systems. The measured (B)H<sup>+</sup>-18C6 BDE of DAP is 52.5 kJ/mol lower than that of IPA and 11.0 kJ/mol higher than that of MGD, consistent with expectations for the measured BDE of DAP.

**Competitive Reaction Pathways.** In most systems examined here, H<sup>+</sup>(18C6) was observed in competition with formation of the protonated base. Because the cross sections for this product are small compared to the most favorable dissociation product, H<sup>+</sup>(B), and the thresholds are higher, it does not significantly influence the kinetics of dissociation for the primary CID pathway. Therefore, a PSL TS was used to analyze the H<sup>+</sup>(B) cross sections in this study. In principle, simultaneous competitive analysis of the H<sup>+</sup>(B) and H<sup>+</sup>(18C6) product cross section would also provide the relative PAs of 18C6 and the bases. However, attempts to analyze the data competitively using a loose PSL TS produced poor fits indicating that there is likely a tight TS barrier that must be overcome to produce the H<sup>+</sup>(18C6) product. Thus, competitive analyses will not provide the desired relative PAs and therefore were not pursued further here.

**Entropy Effects.** The NIST webbook suggests that the PA of 18C6 is 967.0 kJ/mol, higher than the PA of 4MeIMID 952.8 kJ/mol, IMID 942.8 kJ/mol, IPA 923.8 kJ/mol, MA 899.0 kJ/mol, EA 912.0 kJ/mol, NPA 917.8 kJ/mol, and NBA 921.5 kJ/mol. Therefore, the threshold for production of H<sup>+</sup>(18C6) might be expected to be lower than the threshold for dissociation to produce H<sup>+</sup>(B). However, in all of the systems

investigated here, the  $H^+(B)$  product was observed as the major CID product and the lowest energy dissociation pathway. This phenomenon can be understood by considering the change in entropy associated with the dissociation pathways. Entropy effects on CID results have been addressed by McLuckey and Cooks.<sup>85–88</sup> Wesdemiotis and Cerda reported that entropy changes involved in the fragmentation of heterodimers play a critical role in determining the preferred dissociation pathway.<sup>86</sup> For all of the systems examined here, the reaction pathway that involves the formation of  $H^+(B)$  exhibits a greater increase in entropy than the  $H^+(18C6)$  pathway. In the ground-state structure of  $H^+(18C6)$ , the proton is bound to one oxygen atom and stabilized by a hydrogen bonding interaction with another oxygen atom, which results in more constrained rotational and vibration degrees of freedom in the protonated complex of 18C6. Therefore, the relatively favorable entropy change compared to the formation of  $H^+(18C6)$  facilitates the formation of  $H^+(B)$ , making the “apparent” PA of these bases higher than that of 18C6. Therefore, the kinetics of dissociation are severely slowed down, resulting in a more significant kinetic shift as compared to the  $H^+(B)$  pathway. As a result, despite the fact that the reported PA of NBA is 45.5 kJ/mol lower than that of 18C6, the dissociation pathway that forms  $H^+(NBA)$  is still more favorable. Therefore, the  $H^+(NBA)$  and the  $H^+(18C6)$  branching ratio does not accurately reflect the relative PAs of NBA and 18C6 as a result of entropic effects.

The magnitudes of the CID product cross sections for  $H^+(B)$  and  $H^+(18C6)$  are the result of competition between enthalpy and entropy: entropy favors the formation of  $H^+(B)$ , while enthalpy favors the formation of the protonated species that exhibits a higher PA. In the MGD and DAP containing systems, the base exhibits a higher PA than 18C6. Therefore, enthalpy favors the formation of  $H^+(B)$ . The relatively favorable entropy change as compared to the formation of  $H^+(18C6)$  also favors the formation of  $H^+(B)$ . As a result,  $H^+(B)$  was observed as the only CID product. In contrast, in the complexes involving IMID, 4MeIMID, MA, EA, NPA, NBA, and IPA, the PA of the base is lower than that of 18C6. Therefore, enthalpy favors the formation of  $H^+(18C6)$ . However, entropy effects dominate and favor the formation of  $H^+(B)$ . As a result,  $H^+(B)$  was observed as the major CID product and the lowest energy dissociation pathway, while  $H^+(18C6)$  was observed as a very minor competitive CID product.

## CONCLUSIONS

The kinetic energy dependence for CID of nine  $(B)H^+(18C6)$  complexes, where  $B = \text{IMID, 4MeIMID, MA, EA, NPA, NBA, IPA, DAP, and MGD}$ , with Xe is examined by guided ion beam tandem mass spectrometry techniques. For all nine systems, the primary dissociation pathway observed for these noncovalently bound complexes is loss of neutral 18C6. Thresholds for these CID processes are determined after consideration of the effects of the kinetic and internal energy distributions of the reactants, multiple collisions with Xe, and the lifetimes for unimolecular dissociation.  $(B)H^+ - 18C6$  BDEs at 0 K are calculated at the MP2(full), B3LYP, and M06 levels of theory using a 6-311+G(2d,2p) basis set for both levels of geometry optimization, B3LYP/6-31G\* and B3LYP/6-311+G(d,p). Good agreement between MP2(full) and M06 theoretically calculated and TCID experimentally determined BDEs was found in most cases. Compared to MP2(full) theory, M06 theory provides similar (albeit at somewhat reduced) accuracy, but requires significantly less computing time, suggesting that

M06 theory may be a good choice for calculations of larger noncovalently bound systems. The agreement between B3LYP theory and experiment is less satisfactory in these cases, but is better for the primary amines. Geometry optimization with an extended basis set, B3LYP/6-311+G(d,p) does not change the optimized structures, or the computed BDEs significantly, suggesting that the B3LYP/6-31G\* level of theory is sufficient for describing the noncovalently bound systems examined here.

The 18C6 binding affinities determined here combined with structural information obtained from theoretical calculations provides useful insight into the processes that occur in the molecular recognition of 18C6 by peptides and proteins for protein structure and sequence investigation. In the MGD and DAP systems, both enthalpy and entropy favor the formation of  $H^+(B)$ . Therefore,  $H^+(B)$  was observed as the major CID product, and  $H^+(18C6)$  was not observed. In the other  $(B)H^+(18C6)$  complexes, entropy effects dominate the dissociation behavior, resulting in the observation of  $H^+(B)$  as the major and lowest energy CID pathway. However, enthalpy favors the formation of  $H^+(18C6)$ . Therefore,  $H^+(18C6)$  was observed in competition with the primary CID pathway. As a result of the significant difference in entropy for these competitive dissociation pathways, the apparent cross section thresholds of the two products do not necessarily reflect the relative PAs of these bases and 18C6.

The Lys mimic, NBA, and the smaller primary amine analogues exhibit higher binding affinities for 18C6 than the His mimics, 4MeIMID and IMID, and the Arg mimic, MGD, suggesting that among all basic amino acids, the side chains of Lys residues are the preferred binding sites for 18C6 complexation. These results suggest that competition between Arg or His and Lys for 18C6 is not significant. The mimic for the n-terminal amino group, IPA, exhibits a greater 18C6 binding affinity than the Lys mimic, NBA, suggesting that the n-terminus could serve as a favorable alternative binding site for 18C6. Based on correlations between the PA and polarizability of the bases and the measured  $(B)H^+ - 18C6$  BDEs, binding to the n-terminal amino group should be the most competitive with the Lys side chains when the n-terminal amino acid is glycine and should become decreasingly less competitive as the size/polarizability of the side chain increases. This conclusion is being examined in a follow-up to this work by investigating the analogous 18C6 complexes to glycine, alanine, Lys, Arg, and His.

## ASSOCIATED CONTENT

### Supporting Information

Complete citations for refs 49 and 50, tables of vibrational frequencies and average vibrational energies at 298 K, and rotational constants. Figures showing cross sections for CID and thermochemical analysis of zero-pressure extrapolated CID cross sections for the  $(B)H^+(18C6)$  complexes. Ground-state structures of neutral and protonated peptidomimetic bases and 18C6 and the complexes comprised of these species. This information is available free of charge via the Internet at <http://pubs.acs.org/>

## AUTHOR INFORMATION

### Corresponding Author

mrogers@chem.wayne.edu

## ■ ACKNOWLEDGMENTS

This work is supported by the National Science Foundation, Grant CHE-0911191. The authors also thank Wayne State University C&IT for computer time.

## ■ REFERENCES

- (1) Matthews, B. W. *Annu. Rev. Phys. Chem.* **1976**, *27*, 493.
- (2) Dyson, H. J.; Wright, P. E. *Chem. Rev.* **2004**, *104*, 3607.
- (3) Palmer, A. G. *Chem. Rev.* **2004**, *104*, 3623.
- (4) Mendoza, V. L.; Vachet, R. W. *Mass Spectrom. Rev.* **2009**, *28*, 785.
- (5) Wales, T. E.; Engen, J. R. *Mass Spectrom. Rev.* **2006**, *25*, 158.
- (6) Sinz, A. *Mass Spectrom. Rev.* **2006**, *25*, 663.
- (7) Smith, D. L.; Deng, Y.; Zhang, Z. *J. Mass Spectrom.* **1997**, *32*, 135.
- (8) Engen, J. R.; Smith, D. L. *Anal. Chem.* **2001**, *73*, 256A.
- (9) Kaltashov, I. A.; Eyles, S. *J. Mass Spectrom. Rev.* **2002**, *21*, 37.
- (10) Kaltashov, I. A.; Eyles, S. *J. Mass Spectrom. Rev.* **2002**, *37*, 557.
- (11) Hoofnagle, A. N.; Resing, K. A.; Ahn, N. G. *Annu. Rev. Biophys. Biomol. Struct.* **2003**, *32*, 1.
- (12) Eyles, S. J.; Kaltashov, I. A. *Methods* **2004**, *34*, 88.
- (13) Garcia, R. A.; Pantazatos, D.; Villarreal, F. J. *Assay Drug Dev. Technol.* **2004**, *2*, 81.
- (14) Sinz, A. *J. Mass Spectrom.* **2003**, *38*, 1225.
- (15) Brunner, J. *Annu. Rev. Biochem.* **1993**, *62*, 483.
- (16) Kluger, R.; Alagic, A. *Bioorg. Chem.* **2004**, *32*, 451.
- (17) Melcher, K. *Curr. Protein Pept. Sci.* **2004**, *5*, 287.
- (18) Kodadek, T.; Duroux-Richard, I.; Bonnafous, J. C. *Trends Pharmacol. Sci.* **2005**, *26*, 210.
- (19) Back, J. W.; de Jong, L.; Muijsers, A. O.; de Koster, C. G. *J. Mol. Biol.* **2003**, *331*, 303.
- (20) Friedhoff, P. *Anal. Bioanal. Chem.* **2005**, *381*, 78.
- (21) Trakselis, M. A.; Alley, S. C.; Ishmael, F. T. *Bioconjugate Chem.* **2005**, *16*, 741.
- (22) Petrotchenko, E. V.; Pedersen, L. C.; Borchers, C. H.; Tomer, K. B.; Negishi, M. *FEBS Lett.* **2001**, *490*, 39.
- (23) Julian, R. R.; Beauchamp, J. L. *Int. J. Mass Spectrom.* **2001**, *210/211*, 613.
- (24) Julian, R. R.; Beauchamp, J. L. *J. Am. Soc. Mass Spectrom.* **2002**, *13*, 493.
- (25) Julian, R. R.; Beauchamp, J. L. *J. Am. Soc. Mass Spectrom.* **2004**, *15*, 616.
- (26) Julian, R. R.; Akin, M.; May, J. A.; Stoltz, B. M.; Beauchamp, J. L. *Int. J. Mass Spectrom.* **2002**, *220*, 87.
- (27) Julian, R. R.; May, J. A.; Stoltz, B. M.; Beauchamp, J. L. *Int. J. Mass Spectrom.* **2003**, *228*, 851.
- (28) Ly, T.; Julian, R. R. *J. Am. Soc. Mass Spectrom.* **2006**, *17*, 1209.
- (29) Ly, T.; Julian, R. R. *J. Am. Soc. Mass Spectrom.* **2008**, *19*, 1663.
- (30) Liu, Z.; Cheng, S.; Gallie, D. R.; Julian, R. R. *Anal. Chem.* **2008**, *80*, 3846.
- (31) Ly, T.; Liu, Z.; Pujanauski, B. G.; Sarpong, R.; Julian, R. R. *Anal. Chem.* **2008**, *80*, S059.
- (32) Yeh, G. K.; Sun, Q.; Meneses, C.; Julian, R. R. *J. Am. Soc. Mass Spectrom.* **2009**, *20*, 385.
- (33) Wilson, J. J.; Kirkovits, G. J.; Sessler, J. L.; Brodbelt, J. S. *J. Am. Soc. Mass Spectrom.* **2008**, *19*, 257.
- (34) Hossain, M. A.; Schneider, H. J. *J. Am. Chem. Soc.* **1998**, *120*, 11208.
- (35) Pecuh, M. W.; Hamilton, A. D. *Chem. Rev.* **2000**, *100*, 2479.
- (36) Santos, A. M.; Vidal, M.; Pacheco, Y.; Frontera, J.; Báez, C.; Ornellas, O.; Barletta, G.; Griebenow, K. *Biotechnol. Bioeng.* **2001**, *74*, 295.
- (37) Ehrhardm, B.; Misselwitz, R.; Welfle, K.; Hausdorf, G.; Glaser, R. W.; Schneider-Mergener, J.; Welfle, H. *Biochemistry* **1996**, *35*, 9097.
- (38) D'Ambrosio, C.; Talamo, F.; Vitale, R. M.; Amodeo, P.; Tell, G.; Ferrara, L.; Scaloni, A. *Biochemistry* **2003**, *42*, 4430.
- (39) Meot-Ner, M. *J. Am. Chem. Soc.* **1983**, *105*, 4906.
- (40) Sharma, R. B.; Blades, A. T.; Kebarle, P. *J. Am. Chem. Soc.* **1984**, *106*, 510.
- (41) Rodgers, M. T. *J. Phys. Chem. A* **2001**, *105*, 2374.
- (42) Teloy, E.; Gerlich, D. *Chem. Phys.* **1974**, *4*, 417.
- (43) Moison, R. M.; Armentrout, P. B. *J. Am. Soc. Mass Spectrom.* **2007**, *18*, 1124.
- (44) Shaffer, S. A.; Prior, D. C.; Anderson, G. A.; Udseth, H. R.; Smith, R. D. *Anal. Chem.* **1998**, *70*, 4111.
- (45) Shaffer, S. A.; Tolmachev, A.; Prior, D. C.; Anderson, G. A.; Udseth, H. R.; Smith, R. D. *Anal. Chem.* **1999**, *71*, 2957.
- (46) Ervin, K. M.; Armentrout, P. B. *J. Chem. Phys.* **1985**, *83*, 166.
- (47) Dalleska, N. F.; Honma, K.; Sunderlin, L. S.; Armentrout, P. B. *J. Am. Chem. Soc.* **1994**, *116*, 3519.
- (48) *HyperChem Computational Chemistry Software Package*, Version 5.0; Hypercube Inc: Gainsville, FL, 1997.
- (49) Frisch, M. J.; et al. *Gaussian 03*, Revision A.1; Gaussian, Inc.: Wallingford, CT, 2004. See Supporting Information for full reference.
- (50) Frisch, M. J.; et al. *Gaussian 09*, Revision C.01; Gaussian, Inc.: Wallingford, CT, 2009. See Supporting Information for full reference.
- (51) Becke, A. D. *J. Chem. Phys.* **1993**, *98*, 5648.
- (52) Lee, C.; Yang, W.; Parr, R. G. *Phys. Rev. B* **1988**, *37*, 785.
- (53) Foresman, J. B.; Frisch, M. *Exploring Chemistry with Electronic Structure Methods*, 2nd ed.; Gaussian: Pittsburgh, PA, 1996; p 64.
- (54) Boys, S. F.; Bernardi, R. *Mol. Phys.* **1979**, *19*, 553.
- (55) van Duijneveldt, F. B.; van Duijneveldt-van de Rijdt, J. G. C. M.; van Lenthe, J. H. *Chem. Rev.* **1994**, *94*, 1873.
- (56) Muntean, F.; Armentrout, P. B. *J. Chem. Phys.* **2001**, *115*, 1213.
- (57) Beyer, T. S.; Swinehart, D. F. *Commun. ACM* **1979**, *16*, 379.
- (58) Stein, S. E.; Rabinovitch, B. S. *J. Chem. Phys.* **1973**, *58*, 2438.
- (59) Stein, S. E.; Rabinovitch, B. S. *Chem. Phys. Lett.* **1977**, *49*, 183.
- (60) Pople, J. A.; Schlegel, H. B.; Raghavachari, K.; DeFrees, D. J.; Binkley, J. F.; Frisch, M. J.; Whitesides, R. F.; Hout, R. F.; Hehre, W. J. *Int. J. Quantum Chem. Symp.* **1981**, *15*, 269.
- (61) DeFrees, D. J.; McLean, A. D. *J. Chem. Phys.* **1985**, *82*, 333.
- (62) Rodgers, M. T.; Ervin, K. M.; Armentrout, P. B. *J. Chem. Phys.* **1997**, *106*, 4499.
- (63) Khan, F. A.; Clemmer, D. E.; Schultz, R. H.; Armentrout, P. B. *J. Phys. Chem.* **1993**, *97*, 7978.
- (64) Chesnavich, W. J.; Bowers, M. T. *J. Phys. Chem.* **1979**, *83*, 900.
- (65) Yang, Z.; Rodgers, M. T. *J. Phys. Chem. Chem. Phys.* **2004**, *6*, 2749.
- (66) Yang, Z.; Rodgers, M. T. *J. Am. Chem. Soc.* **2004**, *126*, 16217.
- (67) Rannulu, N. S.; Rodgers, M. T. *J. Phys. Chem. Chem. Phys.* **2005**, *7*, 1014.
- (68) Ruan, C.; Rodgers, M. T. *J. Am. Chem. Soc.* **2004**, *126*, 14600.
- (69) Dalleska, N. F.; Honma, K.; Armentrout, P. B. *J. Am. Chem. Soc.* **1993**, *115*, 12125.
- (70) Armentrout, P. B.; Simons, J. *J. Am. Chem. Soc.* **1992**, *114*, 8627.
- (71) Rodgers, M. T.; Armentrout, P. B. *Mass Spectrom. Rev.* **2000**, *19*, 215.
- (72) Glendening, E. D.; Feller, D. *J. Am. Chem. Soc.* **1996**, *118*, 6052.
- (73) Glendening, E. D.; Feller, D.; Thompson, M. A. *J. Am. Chem. Soc.* **1994**, *116*, 10657.
- (74) Rodgers, M. T.; Armentrout, P. B. *J. Phys. Chem. A* **1997**, *101*, 1238.
- (75) Rodgers, M. T.; Armentrout, P. B. *J. Phys. Chem. A* **1997**, *101*, 2614.
- (76) Rodgers, M. T.; Armentrout, P. B. *Int. J. Mass Spectrom.* **1999**, *185/186/187–359*.
- (77) Rodgers, M. T.; Armentrout, P. B. *J. Phys. Chem. A* **1999**, *103*, 4955.
- (78) Armentrout, P. B.; Rodgers, M. T. *J. Phys. Chem. A* **1999**, *104*, 2238.
- (79) Amunugama, R.; Rodgers, M. T. *Int. J. Mass Spectrom.* **2000**, *195/196*, 439.
- (80) Rodgers, M. T.; Armentrout, P. B. *J. Am. Chem. Soc.* **2000**, *122*, 8548.
- (81) Rodgers, M. T.; Armentrout, P. B. *J. Chem. Phys.* **1998**, *109*, 1787.
- (82) Rodgers, M. T. *J. Phys. Chem. A* **2001**, *105*, 8145.
- (83) Kulikov, O. V.; Krestov, G. A. *Pure Appl. Chem.* **1995**, *67*, 1103.
- (84) Hunter, E. P.; Lias, S. G. *J. Phys. Chem. Ref. Data* **1998**, *27*, 413.

(85) McLuckey, S. A.; Cooks, R. G.; Fulford, J. E. *Int. J. Mass Spectrom. Ion Phys* **1983**, *52*, 165.

(86) Cerda, B. A.; Wesdemiotis, C. *J. Am. Chem. Soc.* **1996**, *118*, 11884.

(87) Cheng, X.; Wu, Z.; Fenselau, C. *J. Am. Chem. Soc.* **1993**, *115*, 4844.

(88) Bliznyuk, A. A.; Schaefer, H. F.; Amster, I. J. *J. Am. Chem. Soc.* **1993**, *115*, 5149.